Effect of Acidity and Crystal Morphology of ZSM-5 in Toluene Alkylation with Methyl Mercaptan

Abdelilah Bayout, Claudia Cammarano, Izabel Medeiros Costa, Gleb Veryasov, Tzonka Mineva, Anne Galarneau, Vasile Hulea

Effect of Acidity and Crystal Morphology of ZSM-5 in Toluene Alkylation with Methyl Mercaptan

Abdelilah Bayout,[a] Claudia Cammarano,*[a] Izabel Medeiros Costa,[b] Gleb Veryasov,[c] Tzonka Mineva,[a] Anne Galarneau,[a] and Vasile Hulea[a]

Four H-ZSM-5 zeolites with Si/Al ratios of 15, 25, 40, and 75 and with a number of the acid sites of 0.79, 0.65, 0.43, and 0.29 $mmol_{NH3}\ g_{cat}^{-1}$, respectively, were evaluated in the toluene alkylation by methyl mercaptan. Due to their 3D porous structure and their medium-sized pores, ZSM-5 zeolites were very active and stable against deactivation in this catalytic process. This study shows that the behavior of each catalyst strongly depends on its acidity and crystal morphology, as well as on the reaction parameters. The activity increases with the increase of the concentration of acid sites in the catalysts until 0.43 $mmol_{NH3}\ g_{cat}^{-1}$, and remains almost constant at this maximum (~25%) for the catalysts with higher acidity. When the temperature increased from 375 to 475 °C, the reactant conversions increased, but the catalyst deactivation increased significantly. The selectivity in *para*-xylene was favored by the lower temperature and contact time, but particularly by the morphology of ZSM-5 particles formed by a stacking of thin plate-like shaped crystallites, most probably maximizing pore openings through sinusoidal channels, in which *para*-xylene can freely diffuse, but not *meta*- and *ortho*-xylenes.

1. Introduction

CH_3SH is an abundant contaminant in natural gas and an industrial waste gas. The traditional industrial processes used for removing CH_3SH transform it into dimethyl disulfide, which has not found qualified applications.[1] For economic and ecological reasons, some innovative ways of valorizing the methyl mercaptan have been explored in recent years. Among these, the catalytic conversion of methyl mercaptan into hydrocarbons and H_2S ($CH_3SH \rightarrow$ Hydrocarbons + H_2S) was mainly studied by various groups.[2-11] H_2S produced in this reaction can be recovered by absorption in amines, and then it can be converted into elemental sulfur using the Claus process.

Some studies examined the use of CH_3SH, instead of the widely used CH_3OH[12] and references herein, as an alkylating agent in the alkylation of toluene to produce *para*-xylene,[13,14] the most targeted xylene isomer in industry, a key intermediate in polyethylene terephthalate (PET) production. More than just valorizing a waste, it was demonstrated that CH_3SH can be even more effective than methanol in this reaction. Indeed, using H-ZSM-5 (Si/Al = 15) as a catalyst, the maximum alkylation yield was 67% (450 °C) with CH_3SH, and only 41% with CH_3OH (350 °C).[13] At the same reaction temperature (375 °C), the conversion of toluene was similar using CH_3OH (28%) or CH_3SH (26%), but the conversion of CH_3OH in alkylation was only 33% (65% of methanol was converted in aliphatic hydrocarbons C1-C6), while the conversion of CH_3SH in alkylation was 98% (this value included dimethylsulfide as intermediary product formed acting also as alkylating agent).[14] Therefore, the use of CH_3SH in the alkylation of toluene is highly promising and deserves to be studied more deeply. In the presence of a zeolite with FAU (Y), BEA (β), MFI (ZSM-5), MWW (MCM-22), and MOR topology, the reaction between toluene and CH_3SH followed a Friedel–Crafts mechanism to produce a mixture of aromatics, dominated by xylenes.[14] The pore size/architecture was the crucial parameter for determining the activity and stability of the catalysts. Over zeolites with 12-membered ring channels and/or large cages (i.e., Y, β, MOR, and MCM-22), the main products were the poly-methylbenzenes. Consequently, these zeolites suffered rapid deactivation by coking. In contrast, H-ZSM-5 medium-pore zeolite, composed of straight channels of ellipsoidal cross section (0.52 x 0.56 nm) interconnected with sinusoidal channels of almost circular cross section (0.54 x 0.56 nm) with intersections of the channels giving rise to large cavities of ~0.8 nm,[15] outperformed the other zeolites, exhibiting higher selectivity in alkylation leading to higher selectivity in xylenes and substantially higher resistance to the deactivation.[14] At 375 °C, H-ZSM-5 (Si/Al = 15) allowed to produce with CH_3SH, among xylenes, 40% *para*-xylene, 46% *meta*-xylene, and 14% *ortho*-xylene, hence revealed a higher *para*-selectivity than the thermodynamic equilibrium (24% *para*-xylene, 51% *meta*-xylene, 25% *ortho*-xylene at 375 °C).[14] In comparison, an experiment conducted under identical conditions, in the presence of the same H-ZSM-5 (Si/Al = 15), using CH_3OH as alkylating agent allowed to obtain, among xylenes, 24 % *para*-xylene, 54 % *meta*-xylene, and 22 % *ortho*-xylene.[14] The superior alkylation capabilities and *para*-xylene

[a] Dr. A. Bayout, Dr. C. Cammarano, Dr. T. Mineva, Dr. A. Galarneau, Prof. V. Hulea
ICGM, Univ Montpellier, CNRS, ENSCM, Montpellier, France
E-mail: claudia.cammarano@umontpellier.fr

[b] Dr. I. M. Costa
TotalEnergies OneTech, Courbevoie, France

[c] Dr. G. Veryasov
TotalEnergies OneTech, Zone Industrielle C, Feluy 7181, Belgium

Supporting information for this article is available on the WWW under https://doi.org/10.1002/cctc.202501016

selectivity of CH_3SH suggest the possibility of using this reaction with the dual purpose of valorizing CH_3SH, offering the sustainability benefits of turning a contaminant into a valuable feedstock, and selectively producing *para*-xylene, potentially with higher activity and selectivity compared to CH_3OH, thereby enhancing the process efficiency.

Despite the promising results, prior research was confined to ZSM-5 with Si/Al ratio of 15,[13,14] thereby providing a limited understanding of the influence of catalyst properties on catalytic performance. To fill this gap, the objective of this work is to extend the investigation to other ZSM-5-type catalysts with different Si/Al ratios, acidity and crystal sizes and shapes, in order to identify the optimal properties of ZSM-5 catalysts for maximizing the efficiency and the selectivity to *para*-xylene of the reaction of toluene with CH_3SH. For this purpose, first catalytic tests were conducted over a H-ZSM-5 (Si/Al = 15) catalyst in the 375–425 °C range to identify the optimal reaction temperature. Then, catalytic tests were carried out at 375 °C over different commercial H-ZSM-5 catalysts featuring different Si/Al ratio (Si/Al = 15, 25, 40, and 75) in order to evaluate the influence of their acidity, porosity, crystal morphology on catalytic performance.

2. Experimental Section

2.1. Catalysts

Commercial zeolites NH_4-ZSM-5, named CBV 3024E, CBV 5524G, CBV8014, CBV 15014, with Si/Al ratios of 15, 25, 40, and 75, respectively, were purchased from Zeolyst International. After calcination at 550 °C for 8 h (5 °C/min), the zeolite catalysts were under H^+ form. In the present study, they were denoted as: H-ZSM-5(15), H-ZSM-5(25), H-ZSM-5(40), and H-ZSM-5(75).

2.2. Catalyst Characterization

The crystallinity of the catalysts was examined by X-ray diffraction, in the range 2θ= 4°-50° with an angular step size of 0.0197° and an acquisition time of 0.2 s (Bruker D8 Advance device with a Bragg-Brentano configuration, Bruker Lynx Eye detector, Cu Kα radiation). Nitrogen physisorption measurements were carried out at −196 °C on a Micromeritics Tristar instrument, using samples outgassed under vacuum at 250 °C for 6 h. The specific surface area was determined by using the BET equation taking into account the Rouquerol criteria to choose the pressure domain (Table S1) for the linearity of the equation.[16] The micropore volume and the external surface area were determined by using the *t*-plot method.[16] The morphologies and crystal sizes of zeolites were examined by scanning electron microscopy (SEM, HITACHI instrument). The temperature-programmed desorption of ammonia (NH_3-TPD) was used for evaluating the acidity of the H^+-form zeolites. Before measurement, the materials were slightly compressed (2 t) for 1 min to transform powder into pellets of 16 mm diameter with a press SPECA 15 t and then ground and sieved between 150–250 µm to avoid that NH_3 diffusion is governed by particle size. Before NH_3 adsorption, 50 mg of zeolite was treated under an air flow (30 mL min^{-1}) at 550 °C at 10 °C min^{-1} for 2 h, in a Micromeritics Autochem II apparatus. The pretreated sample was then equilibrated in an ammonia stream (5% NH_3 in He, 45 mL min^{-1}) at 100 °C for 40 min, followed by a purge in helium at the same temperature, until the baseline of the TC detector was stable. Ammonia desorption was carried out under a helium flow (25 mL min^{-1}) at 10 °C min^{-1} up to 600 °C. Temperature ramping starts when the TCD signal is stable and the desorption of weakly physisorbed ammonia is over. A calibration of TCD signal allows data treatment and calculation of the acid sites concentration.

^{27}Al MAS NMR spectra were registered with a VARIAN VNMRS600 spectrometer at 600 MHz ("wide bore" _magnet of 14.1 T). A probe VARIAN T3 MAS was used. ZrO_2 rotors of 3.2 mm diameter were filled with powder and rotated at 22 kHz. The quantitative technique used a single pulse (π/6 of 2 µs) with ^{1}H decoupling and a recycling period of 1 s. The chemical shift was calibrated at 0 ppm with aluminum nitrate. The acquisition window was 192 kHz and a line broadening of 50 or 100 Hz was applied.

2.3. Catalytic Testing

The catalytic alkylation of toluene with methyl mercaptan was performed under atmospheric pressure, in continuous mode, using a stainless-steel plug flow reactor (0.45 cm ID, L=13.6 cm). Prior to the reaction, the catalyst (30 mg, 150–250 µm particle size, mixed with 120 mg of quartz) was activated at 550 °C for 8 h (heating rate of 5 °C min^{-1}) in an air flow. Then, under a nitrogen flow, the catalyst was brought to the reaction temperature. In a typical run, a premixed feed consisting of toluene/CH_3SH/nitrogen =2.5/2.5/95 (mol/mol/mol) was introduced into the reactor with a total flow rate of 30 mL min^{-1}. The complete reactor effluent was analyzed online by gas chromatography, using two apparatus/columns/detectors. The hydrocarbons were analyzed on a Varian 3900, CP-WAX-57-CB (25 m x 0.32 mm x 0.20 µm), FID, while the S-containing compounds were analyzed on a Shimadzu GC 2014, Supel-Q Plot (30 m × 0.32 mm × 0.15 µm), FPD.

3. Results and Discussion

3.1. Catalyst Characterization

The X-ray diffraction (XRD) pattern of the H-ZSM-5 catalysts with Si/Al = 15, 25, 40, and 75 (Figure 1) confirmed the MFI structure of the catalysts used in this study. The relative intensity of the diffraction peaks decreased with the decrease of Al content in H-ZSM-5 catalysts (increase of Si/Al ratio), and the position of the diffraction peak appeared at slightly higher 2 theta angles, which is characteristic of a lower amount of aluminum in the MFI structure. The relative intensity and the position of the diffraction peaks of the catalyst H-ZSM-5(75) were equivalent to the reference ZSM-5 (Si/Al = 200) given in the IZA database (IZA: International Zeolite Association), indicating a low amount of aluminum in the framework.

The nitrogen sorption isotherms at −196 °C of the H-ZSM-5 catalysts were of type I characteristic of microporous materials (Figure S1).[17] The nitrogen adsorption isotherm of H-ZSM-5(75) shows a step at $p/p_0 \sim 0.2$, characteristic of low alumina ZSM-5. This step is due to a densification of the nitrogen molecules with the increase of nitrogen loading in the micropores, described as a transition of "localized fluid-like phase" of nitrogen molecules to "crystalline-like solid phase".[18] In low alumina ZSM-5, the process of volume filling of the micropores does not occur, but rather an adsorption by site within the microporous network. The transition becomes more diffuse with increasing aluminum content, as aluminum creates preferential adsorption sites for

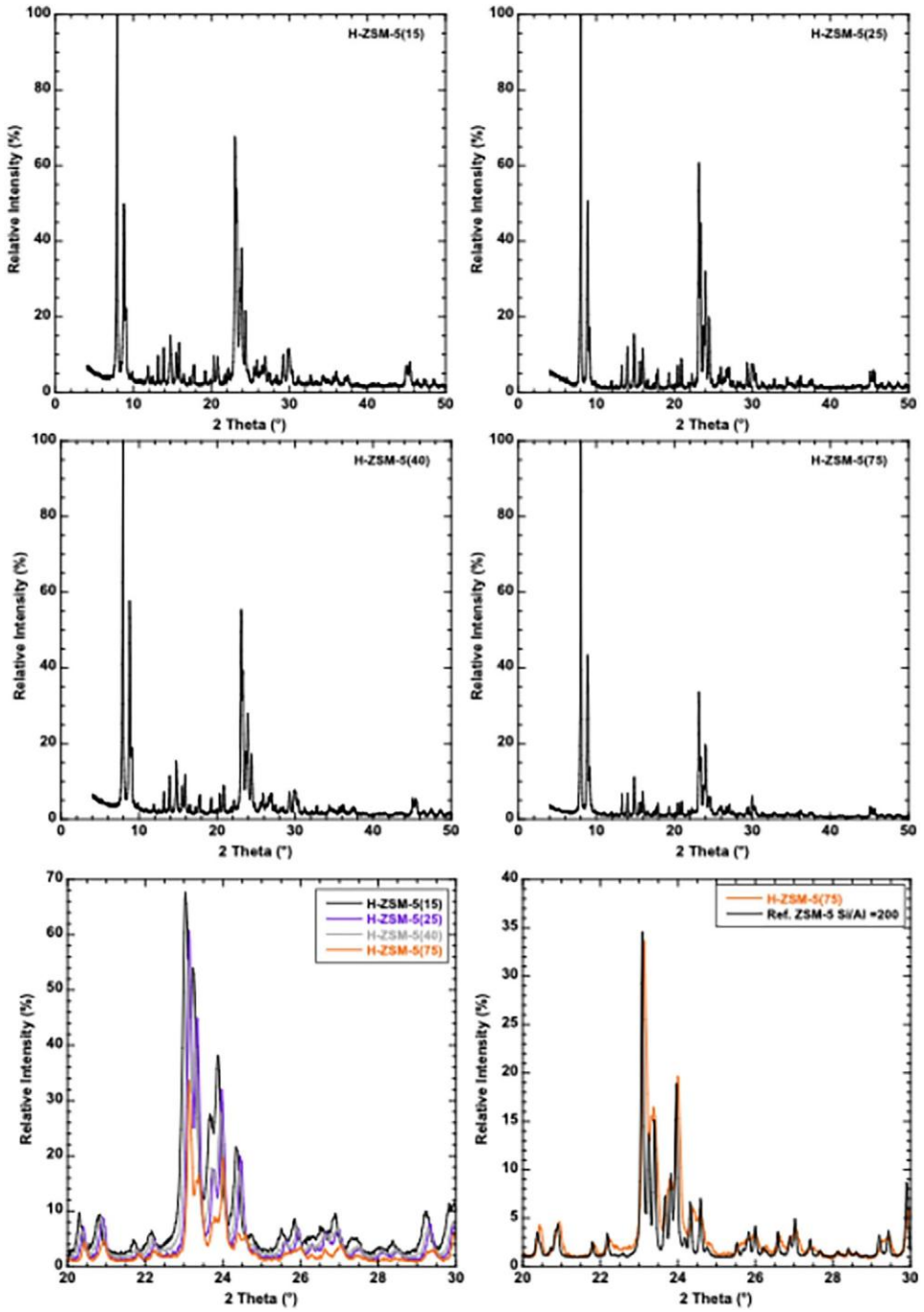

Figure 1. XRD patterns of the H-ZSM-5 zeolite catalysts. Comparison of H-ZSM-5(75) with a reference XRD pattern of ZSM-5 (Si/Al = 200) from IZA database in the range $2\theta = 20^{\circ}$-30°. (IZA: International Zeolite Association, https://www.iza-structure.org/databases/).

quadrupolar molecules as nitrogen, thus creating the "localized fluid-like" phase during the initial adsorption.[18] For example, this nitrogen molecule phase transition is clearly observed for H-ZSM-5(75), still distinguishable for H-ZSM-5(40), and is almost absent for H-ZSM-5(25) and H-ZSM-5(15) (Figure S1). The step due to this transition is better observable in *t*-plot curves (Figure S2). All ZSM-5 contain a "solid-like" nitrogen phase in the plateau region. So micropore volume of ZSM-5 should be determined at the plateau after the phase transition above $p/p_0 = 0.25$. *t*-Plot analysis was used to determine the microporous volume accurately (Figure S2). The change of the slope in the *t*-plot curve above $p/p_0 = 0.25$ occurred for all ZSM-5 at *t* around 0.5 nm, which corresponds to a relative pressure around $p/p_0 = 0.3$ (Figure S2 and Table S1). Micropore volume of all H-ZSM-5 catalysts was around 0.18-0.20 mL g^{-1} (Table 1), which is in agreement with the theoretical micropore volume of MFI structure (0.16 mL g^{-1})[16] and of other synthesized ZSM-5 materials found in literature (0.15-0.19 mL g^{-1}).[19] Theory and simulation study also give the nitrogen accessible surface area of MFI structure and the simulated BET surface area, which are in the range 370-

Table 1. Textural properties of H-ZSM-5 catalysts determined by nitrogen isotherm at 77 K.

	H-ZSM-5(15)	H-ZSM-5(25)	H-ZSM-5(40)	H-ZSM-5(75)
S_{BET} ($m^2\ g^{-1}$)[a]	411	453	443	387
V_{mic} ($mL\ g^{-1}$)[b]	0.176	0.197	0.202	0.177
S_{ext} ($m^2\ g^{-1}$)[b]	63	64	89	68

[a] Determined with the Rouquerol criteria for the upper limit of p/p_0 for the BET equation
[b] Determined by *t*-plot curves analysis

393 $m^2\ g^{-1}$.[16] The H-ZSM-5 catalysts of this study exhibited a BET surface area of 387-453 $m^2\ g^{-1}$ (Tables 1 and S1), which is in agreement with theoretical study and other synthesized ZSM-5 materials found in literature (372-440 $m^2\ g^{-1}$).[19] *t*-Plot analysis was also used to determine the external surface area (S_{ext}) of the H-ZSM-5 catalysts by calculating the slope of the straight line at high *t* of the *t*-plot curves corresponding to $p/p_0 > 0.3$ (Figure S2, Tables 1 and S1). S_{ext} were equivalent for H-ZSM-5(15), H-ZSM-5(25), H-ZSM-5(75) catalysts, with a value of ~65 $m^2\ g^{-1}$, whereas H-ZSM-5(40) exhibits a slightly larger external surface area (89 $m^2\ g^{-1}$) (Table 1).

The nitrogen isotherms of the H-ZSM-5 catalysts also revealed high-pressure hysteresis (Figure S1) usually attributed to inter-particle porosity. Similar H4-type horizontal hysteresis[17] for relative pressure $0.45 < p/p_0 < 1$ with similar height are observed for the catalysts H-ZSM-5(25) and H-ZSM-5(75). This is characteristic of the cavitation phenomenon and is usually attributable to the presence of large embedded pores (>50 nm) connected to the exterior of the particles via pores of diameter < 5 nm, which are most probably the micropores of the zeolites. This type of hysteresis also usually occurs for adsorption between plate-like particles. However, it was demonstrated for ZSM-5 materials that this hysteresis could be due, rather than the existence of mesoporosity in the samples, to swelling mechanisms. This could be ascribed to two different phenomena: swelling of microporous defect regions accessible by large fissures and swelling between parallel crystal « slabs », that is, between two crystal faces acting like plate-like particles.[20] The isotherm of H-ZSM-5(40) revealed the same kind of horizontal hysteresis, typical of cavitation phenomenon, but with a narrower height and a slightly higher slope contributing to a slightly higher external surface area, maybe due to slightly smaller particle aggregates. The high-pressure hysteresis observed in the nitrogen isotherm of the catalyst H-ZSM-5(15) is different. There is no cavitation phenomenon. The hysteresis occurred in relative pressure $0.6 < p/p_0 < 0.9$, with a shape characteristic of large mesopores (~11 nm average diameter), fully accessible from the exterior of the crystals, corresponding to a pore volume of 0.04 $mL\ g^{-1}$. Furthermore, an additional nitrogen adsorption uptake above $p/p_0 > 0.9$ (or t > 0.8 nm in the *t*-plot curve (Figure S2)) was also noticed, which revealed the presence of additional larger pores (>20 nm). These kinds of secondary open porosities in H-ZSM-5(15) catalyst should favor diffusion of reactants and products in catalytic reaction, in contrast to the other H-ZSM-5 catalysts.

To better understand the origin of the high-pressure hysteresis of the nitrogen isotherms of the H-ZSM-5 catalysts, scanning electron micrographs (SEM) were performed to identify the crystals size and morphology (Figure 2). H-ZSM-5(15) features two kinds of crystals: small rounded crystals of 30-50 nm and cubic crystals of 110-130 nm. The voids induced by the aggregation of the smaller crystals explain the first high-pressure hysteresis present at $0.6 < p/p_0 < 0.9$, while the aggregation of the larger crystals is responsible for the nitrogen uptake at $p/p_0 > 0.9$. Differently, H-ZSM-5(40) consists in agglomerates (300-900 nm) built by round crystallites of 60-150 nm. Fissures are clearly identified in between round crystallites. The high-pressure hysteresis of the nitrogen isotherm of H-ZSM-5(40) could therefore come from the swelling of microporous defect regions accessible by these larger fissures, as proposed in literature.[20] H-ZSM-5(25) presents no fissures, but larger hexagonal to rectangular crystals of 150-450 nm, giving rise to cavitation phenomenon, maybe due to swelling between parallel crystal « slabs », that is between two crystal faces acting like plate-like particles.[20] H-ZSM-5(75) consists in agglomerates (750 nm), as H-ZSM-5(40), but which are composed by a stacking of thin plate-like shaped crystallites of 150 nm length, which most probably are responsible for the high-pressure hysteresis due to the swelling between plate-like particles.[20]

Another important characteristic of H-ZSM-5 catalysts is their acidity. The acidity in zeolites is mainly driven by Brönsted acid sites issued of Si-O(H)-Al entities due to the substitution of one tetrahedral Si by one tetrahedral Al. First of all, the total amount of Al present in the commercial zeolites was analyzed by ICP-OES (Tables 2 and S2). This shows a decrease in Al content in H-ZSM-5 catalysts with the increase of Si/Al ratio from 15 to 75, corresponding to a variation of total Al amount of 0.89-0.26 mmol g^{-1}. Then, the amount of tetrahedral Al was determined by ^{27}Al MAS NMR. ^{27}Al MAS NMR (Figure S3) allowed us to calculate the relative amount of tetrahedral aluminum (Al(Td): peak at 55 ppm) and octahedral extra-framework aluminum (Al(Oh): peak at 0 ppm) in the H-ZSM-5 catalysts. Al(Td) species are associated with Brönsted acid sites, Si-O(H)Al in the zeolites, whereas Al(Oh) is attributed to defects on the external surface. The amount of each component was calculated from the percentage of Al(Oh) and Al(Td) determined by ^{27}Al MAS NMR and using the total amount of Al in H-ZSM-5 determined by chemical analysis (Tables 2 and S2). The amount of Al(Oh) in H-ZSM-5 catalysts was low: 0.01 mmol g^{-1} for H-ZSM-5 with Si/Al = 25, 40, 75 and of 0.14 mmol g^{-1} for H-ZSM-5(15) (Table 2). The amount of Al(Td) decreased from 0.75 to 0.25 mmol g^{-1} with the increase of the Si/Al ratio from 15 to 75.

The H-ZSM-5 catalysts' acidity was also measured by NH_3-TPD, which is a technique widely used to characterize catalysts' acidity. The NH_3-TPD profiles (Figure S4) of H-ZSM-5 catalysts feature two desorption peaks centered at 200 and 400 °C, which are usually attributed to weak and strong acidity sites, respectively. The deconvolution of the peaks allows calculating the number of weak, strong, and total acid sites (Table 2). The relative amount of weak and strong acid sites is almost equal for each H-ZSM-5 catalyst and increases with the increase of aluminum content in H-ZSM-5 (decrease of Si/Al ratio). Therefore, the total amount of

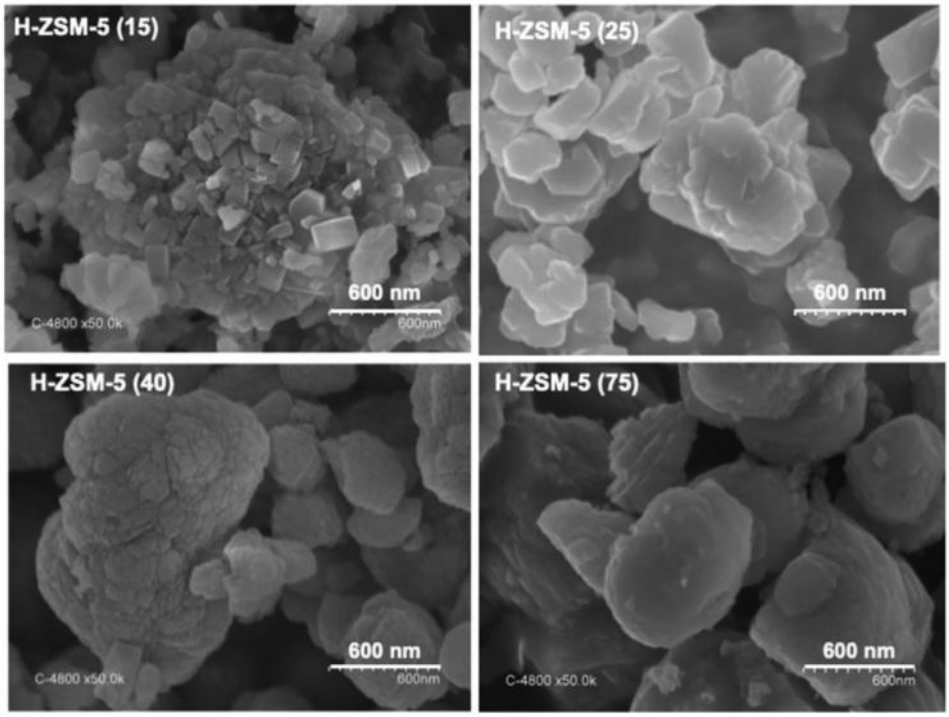

Figure 2. SEM micrographs of H-ZMS-5 zeolite catalysts. Crystal size: H-ZSM5 (15) = 100-250 nm, H-ZSM5 (25) = 200-500 nm, H-ZSM5 (40) = 300-900 nm, H-ZSM5 (75) = 500-750 nm.

Table 2. Acidic properties of H-ZSM-5 catalysts determined by TPD-NH_3, and the amount of Al(Td) and Al(Oh) in H-ZSM-5 catalysts determined by the combination of ^{27}Al MAS NMR and chemical analysis.

	H-ZSM-5(15)	H-ZSM-5(25)	H-ZSM-5(40)	H-ZSM-5(75)
Weak acidity-200 °C ($mmol_{NH3}$ g^{-1})[a)]	0.45	0.34	0.22	0.13
Strong acidity-400 °C ($mmol_{NH3}$ g^{-1})[a)]	0.34	0.31	0.21	0.16
Total acidity ($mmol_{NH3}$ g^{-1})[a)]	0.79	0.65	0.43	0.29
Al (Oh) (mmol g^{-1})[b)]	0.14	0.01	0.01	0.01
Al (Td) (mmol g^{-1})[b)]	0.75	0.69	0.39	0.25
Al Total (mmol g^{-1})[c)]	0.89	0.70	0.40	0.26

[a)] Determined by the deconvolution of the TPD-NH_3 profiles of H-ZSM-5.
[b)] Determined by the deconvolution of the ^{27}Al MAS NMR profiles of H-ZSM-5.
[c)] Determined by ICP-OES of H-ZSM-5 (Table S2).

acid sites in H-ZSM-5 catalysts decreases from 0.79 to 0.29 mmol g^{-1} with the increase of the Si/Al ratio from 15 to 75.

The amount of Al(Td) present in H-ZSM-5 catalysts (Table 2) was compared to the different types of acidity (weak, strong, and total) given by TPD-NH_3 (Figure S5). A very good correlation was obtained between the amount of Al(Td) in the H-ZSM-5 catalysts and the total amount of acid sites determined by NH_3-TPD (Table 2 and Figure S5). Hence, the total acidity of H-ZSM-5 determined by NH_3-TPD corresponds to the Brönsted acid sites of the catalysts and will be used for further correlations with catalytic results.

3.2. Catalytic Alkylation of Toluene by Methyl Mercaptan

3.2.1. Effect of the Temperature

In a previous publication,[14] the alkylation of toluene by methyl mercaptan was performed, in catalytic runs carried out at 375 °C, over zeolites with different topologies: ZSM-5 (Si/Al = 15), FAU-Y (Si/Al = 15), MOR (Si/Al = 10), BEA* (Si/Al = 12.5), MCM-22 (Si/Al = 19) with total acidity of 0.79, 0.46, 1.13, 0.89, 0.62 $mmol_{NH3}$ g^{-1}, respectively. Most of the zeolites showed a strong deactivation over 400 min on stream, except H-ZSM-5 (Si/Al = 15), which maintained the highest and constant conversion of toluene at ~26%.[14]

In the present study, the behavior of H-ZSM-5(15) zeolite was examined at various temperatures. The alkylation reaction was carried out under the following conditions: catalyst mass = 30 mg, WHSV = 9.4 $g_{toluene+CH3SH}$ g_{cat}^{-1} h^{-1}, toluene/methyl mercaptan = 1/1, and atmospheric pressure. The catalytic tests were performed at 375, 425, and 475 °C for 400 min on stream. The effect of the temperature on the conversion of the two reactants is shown in Figure 3.

These results show a significant effect of the temperature on the catalytic activity, particularly on the toluene conversion, which increased from 27% to 77% between 375 and 475 °C. As previously noticed at 375 °C,[14] the reagent conversions did not vary over the reaction time, but they slightly decreased at higher temperatures, indicating a low deactivation of the H-ZSM-5(15) catalyst.

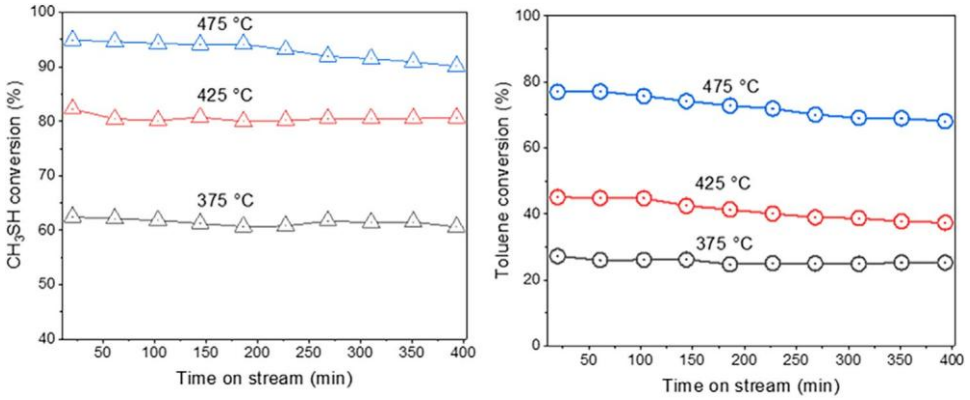

Figure 3. Temperature effect on the conversion of methyl mercaptan (left) and toluene (right) on H-ZSM-5(15) catalyst. Conditions: m_{cat} = 30 mg; toluene/CH_3SH = 1/1; WHSV = 9.4 $g_{toluene+CH3SH}$ g_{cat}^{-1} h^{-1}.

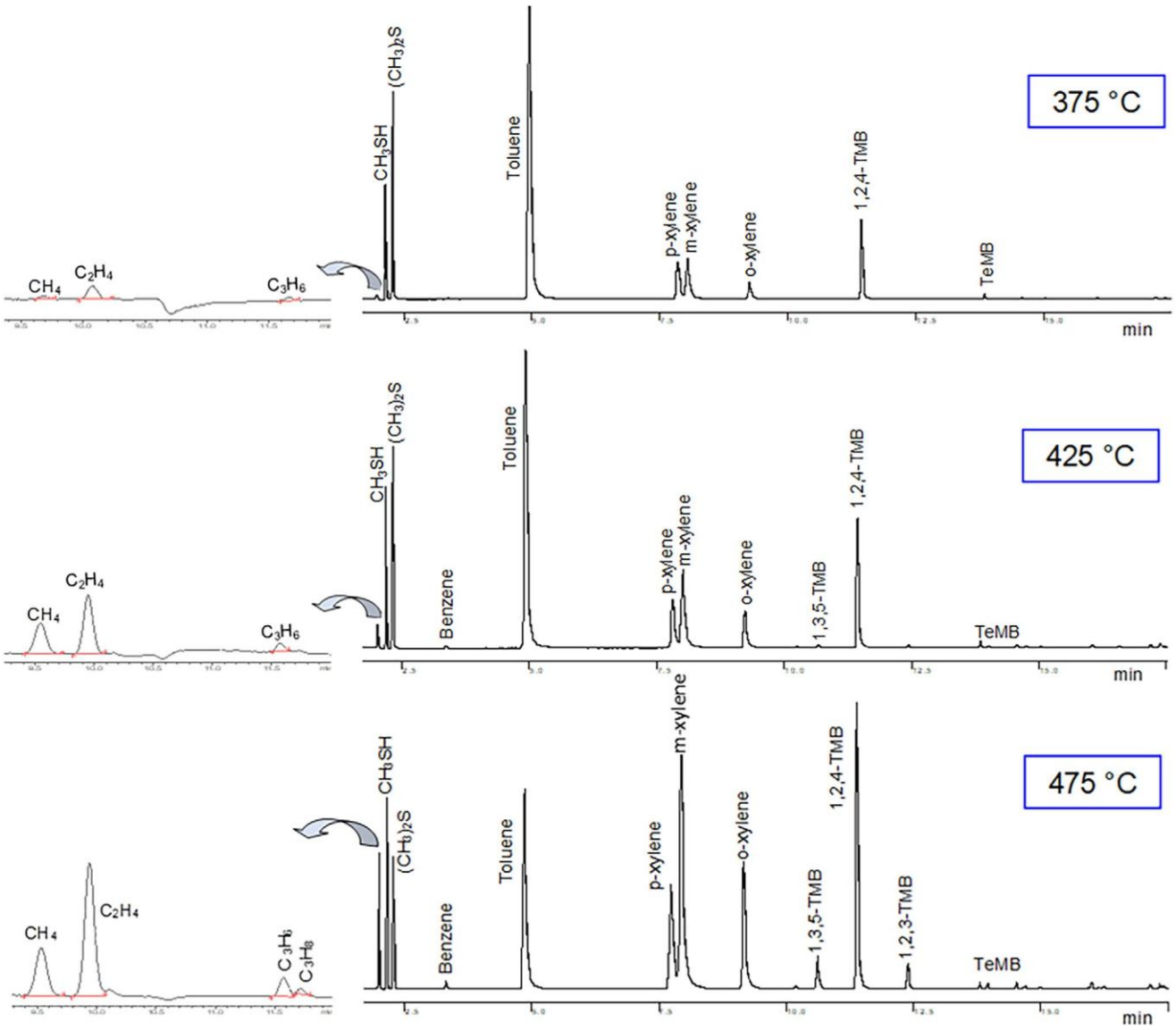

Figure 4. GC-FID chromatograms for the reaction between toluene and CH_3SH on H-ZSM-5(15). Conditions: m_{cat} = 30 mg, volume flow rate = 30 mL min^{-1}, toluene/CH_3SH = 1/1, WHSV = 9.4 $g_{toluene+CH3SH}$ g_{cat}^{-1} h^{-1}, tos = 60 min.

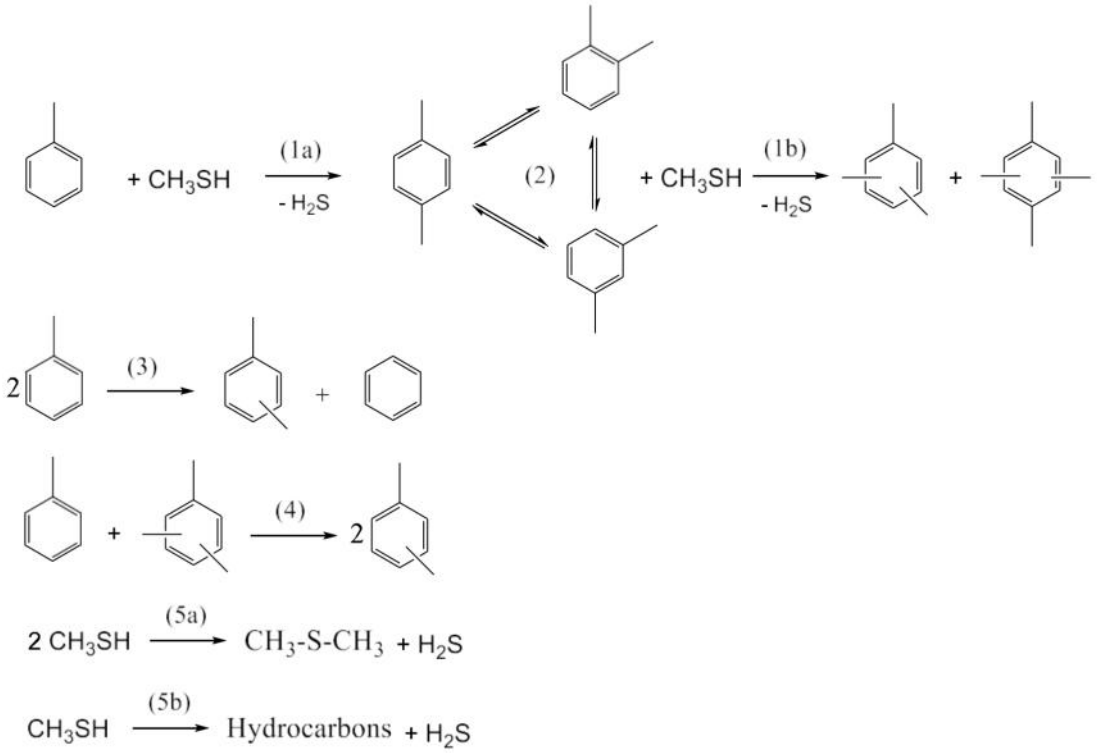

Scheme 1. Reactions involved in the process: (1a) toluene and xylenes, (1b) alkylation, (2) xylenes isomerization, (3) toluene disproportionation, (4) toluene-trimethylbenzene transalkylation, (5a) and (5b) methyl mercaptan conversion into dimethyl sulfide or hydrocarbons.

Figure 4 shows the nature of the products obtained at different temperatures. The molecules produced at 425 °C are not very different from those obtained at 375 °C. Thus, dimethyl sulfide (DMS) and methylbenzenes are the major products, while the amount of light hydrocarbons is insignificant. In contrast, at 475 °C, a high decrease in DMS (Figures 4 and S6) was observed, proving that this primary product is highly involved in the toluene alkylation and/or decomposition into light hydrocarbons.

In order to explain the formation of the products shown in Figure 4, a series of reactions must be considered (Scheme 1). Note that these reactions are similar to those usually observed in the toluene alkylation by methanol over zeolites.[21]

In all tests, xylenes and trimethylbenzenes are the major methylaromatics, while the amount of tetramethylbenzenes was lower than 1.5%. The ratio between xylenes and TMBs slightly increased when the temperature increased (Figure 5). This could be explained by considering the transalkylation reaction between toluene and TMBs (Scheme 1), which is favored at high temperatures.[22]

The distribution of xylene isomers was highly dependent on the temperature. As shown in Figure 6 and Table 3, the *para*-xylene (para-X) selectivity decreased from 37% to 24% when the temperature increased from 375 to 475 °C. The distribution of xylenes at 475 °C is comparable to that expected for the thermodynamic equilibrium (i.e., para-X: meta-X: ortho-X = 24:51:25).[21]

As shown in Figure 4, only a small amount of benzene was formed, suggesting that the toluene disproportionation is insignificant. According to literature,[23-25] this reaction mainly

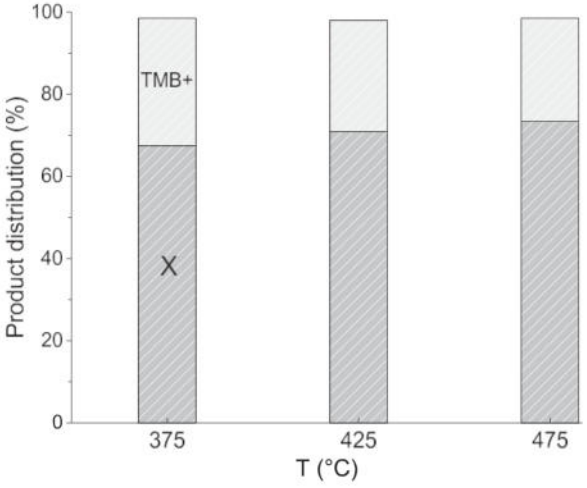

Figure 5. Aromatic distribution as a function of temperature for the reaction between toluene and CH_3SH on H-ZSM-5(15) (X = xylenes, TMB^+ = tri- and tetra-methylbenzenes).

Table 3. The effect of the temperature on the toluene conversion and xylenes distribution for the reaction between toluene and CH_3SH on H-ZSM-5(15).

Temperature (°C)	375	425	475
Toluene conversion (%)	27	46	78
Xylenes selectivity (%)			
para-X: meta-X: ortho-X	37:47:16	28:52:20	23:54:23

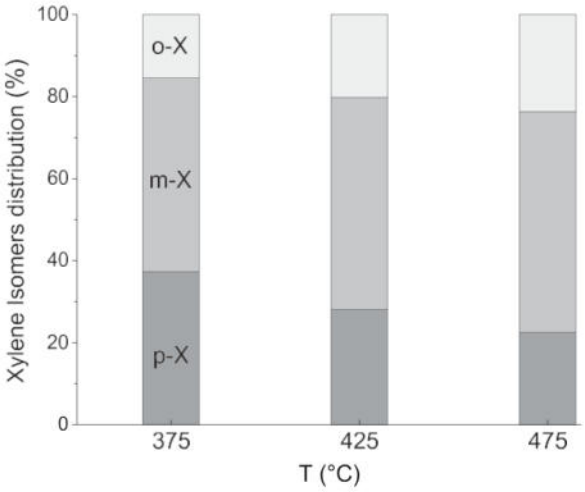

Figure 6. Distribution of xylenes (X) as a function of temperature for the reaction between toluene and CH_3SH on H-ZSM-5(15) (o = ortho, m = meta, p = para).

takes place through a bimolecular mechanism, which is favored by the presence of large pores and cages in zeolites. The porosity of H-ZSM-5 zeolite is not able to accommodate the large molecules.

Due to the high conversion of toluene obtained at high temperature, the yields of alkylation and xylenes sharply increased with the temperature (Figure 7). The effect of the temperature on the para-xylene yield was weaker. It should be noted that the distribution of aromatics, as well as their yields, practically did not change during the 400 min of reaction.

At 375 and 425 °C, only small quantities of C1-C3 hydrocarbons were produced (Figure 4). In contrast, at 475 °C, the quantity of these hydrocarbons was greater. Ethylene and propylene were formed in much greater quantities compared to C1-C3 unsaturated hydrocarbons. This result was compared with that obtained in a catalytic test in which methyl mercaptan alone was fed through the reactor. As observed in Figure 8, only small amount of light hydrocarbons were formed. Among them, methane (an unsaturated hydrocarbon) was quantitatively more important than ethylene. Some aromatic hydrocarbons, such as toluene, xylene and trimethylbenzene were also formed.

In order to describe the formation of the hydrocarbons presented in Figure 8, it will be assumed that the mechanism of transformation of methyl mercaptan into hydrocarbons is similar to that proposed for the conversion of methanol into hydrocarbons (MTH). For this reaction, there is a general consensus that the light olefins like ethylene and propylene are the result of a so-called "Hydrocarbon Pool" (HP) mechanism.[26] According to this mechanism, the aromatic species trapped in the pores/cages of the zeolites undergo successive stages of methylation by methanol and eliminate the light alkenes.

When methyl mercaptan alone was fed through the reactor, the H-ZSM-5 catalyst (a 3D porous zeolite) allowed the diffusion of the methylbenzenes formed in reaction towards the product flow, avoiding the accumulation in its pores of the HP active species (responsible for the formation of light olefins).[27] The formation of unsaturated aliphatic hydrocarbons and of aromatics is due to the hydrogen transfer reactions, favored at high temperature. In contrast, when toluene and methyl mercaptan are fed together into the reactor (Figure 4), the abundance of toluene in the pores of the catalyst can activate the so-called "Aromatics Carbon Pool" cycle, and thus the formation of light olefins through an HP mechanism.[28,29]

According to Scheme 1 and Figure 4, methyl mercaptan was consumed in three reactions. A significant part was transformed into dimethyl sulfide, a part into xylenes and trimethylbenzenes, and a very small amount was transformed into light aliphatic hydrocarbons. If methyl mercaptan and dimethyl sulfide are treated as a single alkylating agent (because dimethyl sulfide is also an alkylating agent, as shown in Ref. [14]), it can be stated that the fraction of the methyl mercaptan involved in the toluene alkylation (called alkylation efficiency) varied from 90% to 98%. Note that these values are superior to most of those reported in literature for the toluene alkylation with methanol in the presence of zeolites, under comparable process parameters.[30] This drawback in the toluene alkylation with methanol is a major challenge for the development of industrial applications, and hence, the use of methyl mercaptan opens up new perspectives.

3.3. Effect of the Zeolite Acidity and Crystal Morphology

Then, the influence of the acidity of H-ZSM-5 catalyst in the toluene alkylation with methyl mercaptan was examined. Four H-ZSM-5 catalysts with different Si/Al ratio were selected: H-ZSM-5(15), H-ZSM-5(25), H-ZSM-5(40), and H-ZSM-5(75) catalysts featuring an amount of total acid sites, determined by NH_3-TPD, of 0.79, 0.65, 0.43, and 0.29 $mmol_{NH3}\ g_{cat}^{-1}$, respectively (Table 2). The reaction between toluene and methyl mercaptan was carried out under the following conditions: catalyst mass = 30 mg, T = 375 °C, volume flow rate = 30 mL min^{-1}, toluene: CH_3SH = 1:1 and WHSV = 9.4 $g_{toluene+CH3SH}\ g_{cat}^{-1}\ h^{-1}$. Figure S7 shows the toluene conversions and the xylene and para-xylene selectivity as function of total acidity. The conversion, which did not vary during the catalytic runs, increased from 10% to 25% with the increase of the concentration of acid sites in the catalysts from 0.29 to 0.43 $mmol_{NH3}\ g_{cat}^{-1}$ (for H-ZSM-5(75) and H-ZSM-5(40), respectively) and remained almost constant at this maximum (~25%) for the catalysts with higher acidity (H-ZSM-5(15), H-ZSM-5(25)). Similarly, the selectivity to xylenes (i.e., the amount of xylenes among the methylbenzenes), decreased from 88% to 71% when the concentration of acid sites increased from 0.29 to 0.43 $mmol_{NH3}\ g_{cat}^{-1}$ (for H-ZSM-5(75) and H-ZSM-5(40), respectively) (Figures 9 and S7), then it remains almost invariable (~70%) for the catalysts with higher acidity (H-ZSM-5(15), H-ZSM-5(25)). In other words, a higher acidity favors the polymethylation of toluene, so lower xylenes formation. The increase of toluene conversion with the catalyst acidity followed by a plateau of toluene conversion for acidity higher than 0.43 $mmol_{NH3}\ g_{cat}^{-1}$ (Figure S7) is not proper to CH_3SH as the same behavior was observed by using the same catalysts and CH_3OH as alkylating agent in other conditions (Figure S8).[12] Furthermore, the same correlation was obtained with mesoporous ZSM-5, of different

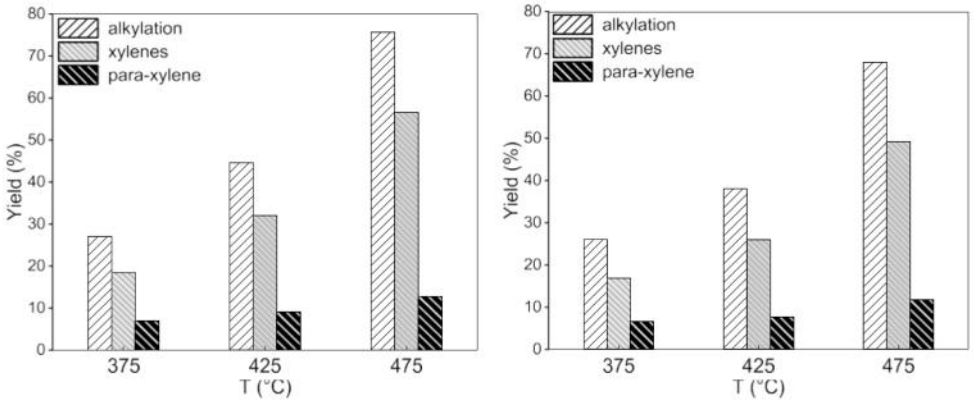

Figure 7. Effect of the temperature on the yields in alkylation, xylenes and para-xylene, at 20 min (left) and at 400 min on stream (right), for the reaction between toluene and CH_3SH on H-ZSM-5(15).

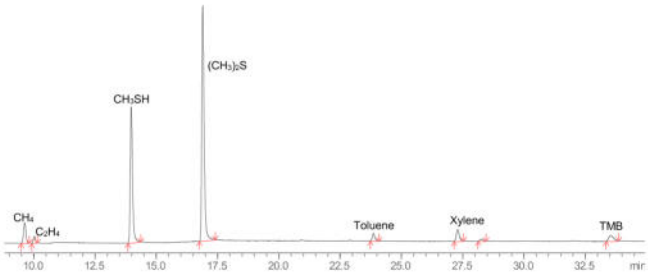

Figure 8. GC-FID chromatogram for the CH_3SH decomposition on H-ZSM-5(15). Conditions: T = 475 °C, m_{cat} = 30 mg, volume flow rate = 30 mL min^{-1}, WHSV = 3.2 g_{CH3SH} $gcat^{-1}$ h^{-1}, tos = 60 min.

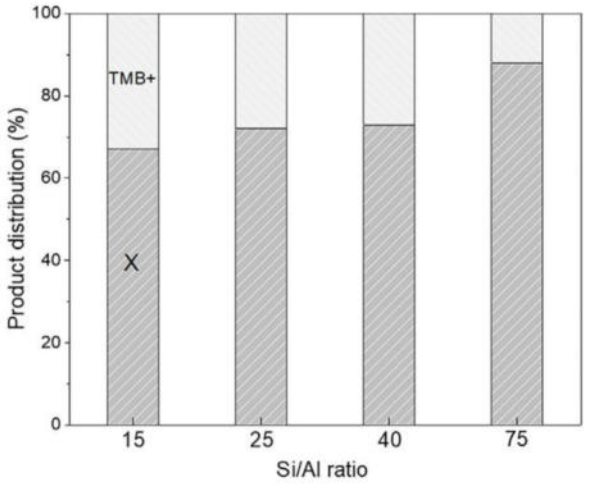

Figure 9. Effect of the Si/Al ratio of H-ZSM-5 catalysts (H-ZSM-5(15), H-ZSM-5(25), H-ZSM-5(40), H-ZSM-5(75)) on the product distribution for the reaction between toluene and CH_3SH (X = xylenes, TMB_+ = tri- and tetra-methylbenzenes).

acidity and increasing mesopore volume. Since the plateau was observed independently of the presence of mesopores, providing faster diffusion of reactants and products, hence with less diffusion limitation,[12,31] the existence of a plateau is most probably due to the saturation of the acid sites by CH_3SH rather than diffusion limitations.

Indeed, for CH_3OH, the main steps in the mechanism of alkylation are: (i) adsorption of CH_3OH on a Brönsted proton; (ii) dehydration of CH_3OH to form surface-bound methoxy species Al-O(CH_3)-Si, and (iii) methylation, involving the interaction of the methoxy function with toluene. DFT calculation showed that the methylation of toluene by methanol on ZSM-5 to form xylene isomers occurs through similar transition states and activation barriers.[32] Methylation was found to be the rate-determining step, with the highest free-energy barrier (88 kJ mol^{-1}), the isomerization had an activation free energy of 34 kJ mol^{-1}. The formation of grafted methoxy group at the surface of the pores is fast, whereas the methylation of toluene is slower.[33] For CH_3SH as an alkylating agent for toluene, the mechanism should be the same, as the correlation between toluene conversion and acidity is similar for CH_3SH and CH_3OH (Figures S7 and S8). For CH_3SH, the kinetic constants were experimentally calculated for H-ZSM-5(15) as catalyst and were (1.6 h^{-1} at 375 °C, 2.5 h^{-1} at 400 °C and 4.2 h^{-1} at 425 °C) corresponding to an apparent activation energy of 80 kJ mol^{-1},[32] close to the activation energy of the alkylation using MeOH (88 kJ mol^{-1}).[33]

The most significant result of the present study is the distribution of xylenes (Figure 10). The *para*-xylene selectivity exhibited by H-ZSM-5(15), H-ZSM-5(25), and H-ZSM-5(40) is 37%, 41%, and 34%, respectively, whereas an outstanding 75% *para*-xylene selectivity is reached with H-ZSM-5(75) catalyst (Figures 10 and S7), surpassing other catalysts. Note that the xylene distributions did not change during the 400 min of reaction.

Since the catalytic tests were carried out using the same mass of catalysts (i.e., 30 mg), the amounts of the acid sites in the reactor were 23.7, 19.2, 12.9, and 8.7 µmol for H-ZSM-5(15), H-ZSM-5(25), H-ZSM-5(40), and H-ZSM-5(75), respectively. Thus, a first explanation for the high *para*-xylene selectivity revealed by H-ZSM-5(75) could be related to the lower number of acid sites present in the reactor. To verify this assumption, a catalytic test under "iso-acidity" conditions was carried out. In order to put into the reactor the same amount of acid sites, a test was performed using 14 mg of H-ZSM-5(25), corresponding to 8.7 µmol of acid sites in the reactor, as for 30 mg of H-ZSM-5(75). The results obtained are shown in Figure 11.

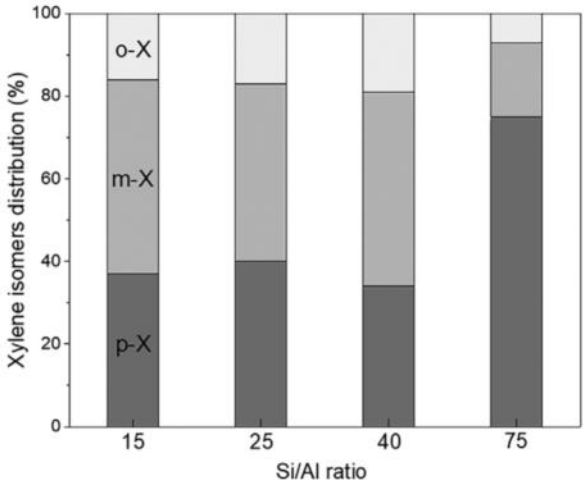

Figure 10. Effect of the Si/Al ratio of H-ZSM-5 catalysts on the xylene (X) distribution for the reaction between toluene and CH_3SH(o = ortho, m = meta, p = para).

The differences between the toluene conversion obtained over the two catalysts were not significant (Figure 11). In contrast, the distributions of the aromatic products were very different. Despite the same amount of acid sites in the reactor, H-ZSM-5(75) catalyst featured a higher xylene selectivity (88%) and *para*-xylene selectivity (75%) compared to H-ZSM-5(25), although the latter showed a slight increase in xylene selectivity from 72% to 82% and in *para*-xylene selectivity from 40% to 50% (Figures 9-11 and S7). This means that the *para*-xylene selectivity can be improved up to a certain level by reducing the number of the acid sites in the reactor, but this is not enough to explain the experimental results of high *para*-xylene selectivity (75%) obtained with H-ZSM-5(75).

To better understand the *para*-selectivity, the pore channels of ZSM-5 and the size of the molecules have been considered. Olson et al.,[34] calculated the framework topology of an as-synthesized ZSM-5 (Si/Al = 86) containing Na^+ and TPA^+ cations by single crystal XRD. The 3D channel system of ZSM-5 consists of straight channels running parallel to [010] having 10-member rings of ca. 0.54 × 0.56 nm free diameter and sinusoidal channels running parallel to [100] having 10-member ring openings of ca. 0.51 × 0.54 nm. As comparison, by using the framework of MFI structure (without cations) given in the database of IZA structures, the sizes of the pore channels were measured using the software VESTA[35] from center of opposite oxygen atoms: straight channel (along *b*-axis) 0.78 × 0.81 nm and sinusoidal channel (along *a*-axis) 0.80 × 0.82 nm. By adding ionic radii of oxygen atoms of 0.135 nm, as proposed by Olson et al.,[34] the free diameter of the two channels became for straight ellipsoidal channel 0.51 × 0.54 nm (along *b*-axis) and for sinusoidal circular channel (along *a*-axis) 0.53 × 0.55 nm. Liu et al.[36] synthesized coffin-like shape ZSM-5 crystals of width of 250 nm along *a*-axis, thickness of 100 nm along *b*-axis and length of 550–1500 nm along c-axis. According to transmission electron microscopic (TEM) and aberration-corrected scanning transmission electron microscopic (STEM) images, the pores of the straight channels that run along *b*-axis can be distinguished along [010] plane and features openings of ~0.53 nm, while the pores of sinusoidal channels that are parallel to *a*-axis could be observed along the [100] plane and featured smaller openings of ~0.42 nm. On such plate-like crystals, straight channels openings are therefore on the top of the plates and sinusoidal openings on the side or thickness of the plates. On STEM images, openings of sinusoidal channels appeared clearly smaller than openings of straight channels. Hernandez et al.,[37] proposed also a simple geometrical representation of the ZSM-5 pore network with straight main channels of ovoid section (0.51 × 0.57 nm) separated by a distance of 0.665 nm by perpendicular porous cylindrical connections of 0.54 nm circular section, which are themselves dispatched regularly along the main channel by a distance of 0.45 nm. This representation allows to calculate geometrically the volume of the main straight channels in comparison to the total pore volume (main straight channel and cylindrical connections). Hence, the main straight channels represent 60% of the total pore volume, and the cylindrical connecting pores 40%.

Although ZSM-5 features pore diameter of ~0.55 nm, this zeolite can readily adsorb large molecules as *o*- and *m*-xylene, 1,2,4-trimethylbenzene, naphthalene, all having a kinetic diameter of ~0.69 nm.[34] The kinetic diameter of *p*-xylene is slightly smaller (0.585 nm).[38] Penta-methylbenzene and 1,3,5-trimethylbenzene (~0.78 nm) are essentially excluded. Some modeling was performed to estimate the critical dimensions of xylenes in high silica zeolites by Courtal space-filling models.[39] For molecules as *o*-, *p*-xylenes, benzene, *n*-hexane, this model-

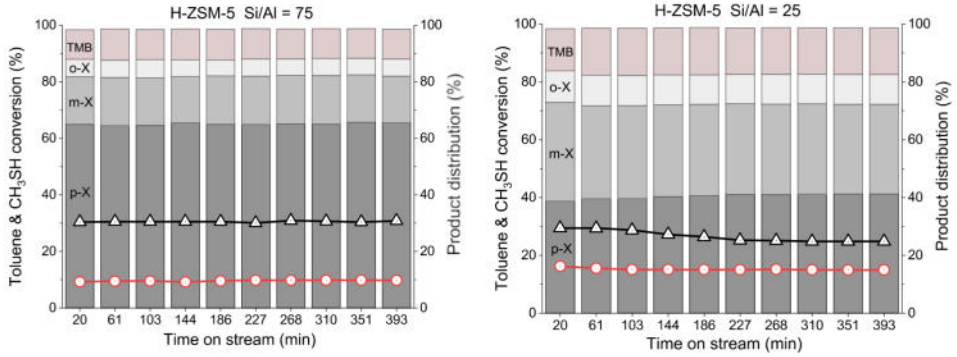

Figure 11. Catalytic results on toluene alkylation with methyl mercaptan obtained at 375 °C, with 30 mg of H-ZSM-5(75) (left) and 14 mg of H-ZSM-5(25) (right). The red curve (circles) is the conversion of toluene, and the black curve (triangles) is the conversion of methyl mercaptan.

ing evaluated their dimensions as: 0.41 × 0.69 × 0.91 nm, 0.37 × 0.62 × 0.86 nm, 0.34 × 0.62 × 0.69 nm, 0.39 × 0.43 × 0.91 nm, respectively, so widths for *p*-xylene of 0.62 nm and 0.69 nm for *o*-xylene. The size of the single molecules of the reaction was also evaluated using the software VESTA[35] as comparison. The width and length of toluene and *o*-(or *m*-) xylene, *p*-xylene were calculated from center of opposite H atoms and corresponded to: 0.177 × 0.430 × 0.586 nm, 0.177 × 0.469 × 0.599 nm, 0.177 × 0.430 × 0.695 nm, respectively (Figure S9). Density functional theory (DFT) calculations, detailed in the reference of Mineva et al.,[40] show that hydrogen atoms in xylenes carry a partial positive charge. The aromatic ring hydrogens have charges of about +0.25 e, while the methyl hydrogens carry approximately +0.1 e. Given that H^+ has an ionic radius close to zero[41] and neutral hydrogen has an atomic radius close to 0.05 nm,[42] the ionic radii of $H^{+0.25}$ and $H^{+0.1}$ was estimated to be approximately 0.03 and 0.04 nm, respectively. Hence, the final sizes of the molecules became: 0.257 × 0.490 × 0.656 nm, 0.257 × 0.539 × 0.669 nm, 0.257 × 0.490 × 0.775 nm, for toluene and *o*-(or *m*-) xylene, *p*-xylene, respectively (Figure S9). Toluene and *p*-xylene featured the same width (0.49 nm), whereas *o*- and *m*-xylene are larger molecules with 0.54 nm width.

Despite the width of xylenes isomers is similar to the pore size of ZSM-5 channels, they can readily diffuse into the pores of ZSM-5, as high adsorption capacities were reported in literature.[43] The flexibility of the molecules and the non-rigidity of the pore structures should be taken into account.[39] It was shown that in presence of *p*-xylene the pore openings of ZSM-5 straight channels (0.51 × 0.57 nm) were distorted to 0.62 × 0.48 nm.[38] ZSM-5 adsorbed similar amounts of *o*-, *m*-, *p*-xylenes, benzene, and *n*-hexane with adsorption capacities of 93.3, 94.3, 127.2, 104.5, and 117.0 mg g^{-1}, respectively.[43] By using densities of the liquids of 0.871, 0.860, 0.850, 0.878, and 0.650 g cm^{-3},[34] for *o*-, *m*-, *p*-xylenes, benzene, *n*-hexane, respectively, these adsorption capacities correspond to volumes of 0.107, 0.110, 0.149, 0.119, and 0.180 mL g^{-1}. The theoretical and experimental pore volume of ZSM-5, determined with nitrogen as a probe, is 0.15-0.16 mL g^{-1}.[16] Hence, these results showed that *p*-xylene filled entirely the pore volume of ZSM-5, while *o*-/*m*-xylenes occupied 73% of the pore channels. This reflects the exclusion of *o*-/*m*-xylenes from certain regions of the pores of ZSM-5. As *o*- and *m*-xylenes can only diffuse through straight channels,[44] the regions of exclusion in ZSM-5 for *o*- and *m*-xylene correspond to a part of the sinusoidal channels. Considering the simple geometrical model of ZSM-5 pore network of Hernandez,[37] *o*-/*m*-xylene would occupy 100% of the main straight channels and 32% of the cylindrical connections (16% on each extremity), which corresponds to a penetration of only 0.110 nm on each side of the perpendicular cylindrical connections of 0.665 nm length. The *o*- and *m*-xylene are not present in cylindrical connections. Only *p*-xylene can diffuse through sinusoidal channels. The diffusion of *p*-xylene is faster in straight channels than in sinusoidal channels.[44] Globally, the diffusion of *p*-xylene in ZSM-5 ($\sim 10^{-7}$ cm^2 s^{-1}) is 1000 times superior to that of *o*-/*m*-xylenes ($\sim 10^{-10}$ cm^2 s^{-1}).[34] Sinusoidal channels are more efficient for xylene isomers shape/size sieving, as *o*- and *m*-xylenes do not diffuse in sinusoidal channels.[45]

Even if *p*-xylene diffuses in both channels, isomerization of *p*-xylene into *m*- and *o*-xylene can occur on the external surface of the crystals, often leading to a thermodynamic equilibrium composition of *p*-/*m*-/*o*-xylene of 24:52:24%.[46] Hence, strategies to maximize *p*-xylene selectivity were proposed and verified: (i) to limit the number of acid sites at the external surface of ZSM-5 crystals, (ii) to design ZSM-5 crystal with dominantly exposure, on its external surface, of [100] facets (where sinusoidal channel openings are exposed), (iii) to locate Al preferentially in the channels (and not in the cavity located at the channels intersections) where only *p*-xylene can be formed (*o*- and *m*-xylene being formed in the cavities of channels intersections (~0.8-0.9 nm) due to their size). The first route was achieved simultaneously as the second route by synthesizing ZSM-5 crystals with low Al concentration at the external surface (with an inverse gradient of Al concentration in the crystal as in usual synthesis of ZSM-5) and by designing big coffin-like shape crystals of 6 μm thickness (exposure [010] and [100] facets with openings through sinusoidal channels) and 15-25 μm length, 7-10 μm width (top of the crystal ([010] facet with pore openings of straight channel) which was covered by a thin intergrowth crystal featuring [100] facet, corresponding to openings through sinusoidal channels.[45] This ZSM-5 synthesis was performed using a mixture of structure directing agents (SDA) as n-butylamine/TPA^+ = 7.8 and reached 99% *para*-selectivity in the alkylation of toluene by CH_3OH.[45] The third route was achieved by using a mixture of SDA, ethylenediamine/TPA^+ = 15, which favors Al position in the channel (and not in the cavity located at the channels intersections) and allowed 80% of *para*-selectivity.[47] The selectivity of *p*-/*m*-/*o*-xylene was 80:1:19%, while a selectivity of 30:5:65% was found for Al located only in the cavity of channel intersections (by using only TPA^+ as SDA) at 2% conversion of toluene. Controlling the morphology of ZSM-5 zeolite is of considerable importance for the diffusion and shape-selective catalysis.[36] Maximizing [010] facets (openings through straight channel) would favor diffusion and diminish internal coke in cracking reactions,[36] while maximizing [100] facets (openings through sinusoidal channel) would favor shape selectivity towards smallest molecules as p-xylene in the alkylation of toluene by CH_3OH or CH_3SH. As plate-like morphology crystals of 100 nm thickness feature [010] facets on the top of the plate[36] (openings through straight channels), a stacking of thin plate-like morphology at the top of each other would expose mainly the sides of the stacking composed therefore of [100] facets[36] and hence would maximize pore openings through sinusoidal channels.

H-ZSM-5(75) exhibits this unusual stacking of thin plate-like morphology (Figure 2), hence this particular morphology could be most probably at the origin the high *para*-selectivity (75%) of this catalyst. Being a commercial catalyst, it was most probably synthesized using TPAOH and NaOH, and not specific SDA, as butylamine[45] or ethylene diamine,[47] to direct the location of Al at the surface of the crystal and/or in the channels (and not in the cavities located at the channels intersections). Additionally, a similar morphology (a stacking of plate-like shaped crystallites) was obtained in macroporous ZSM-5 monoliths synthesized

with a mixture of TPAOH and NaOH, and these monoliths featured also a remarkable high *para*-selectivity of 68%–81% in the alkylation of toluene by CH_3OH in other reaction conditions.[48] The high *para*-selectivity of H-ZSM-5(75) catalyst is not specific to the use of CH_3SH as a similar high *para*-selectivity (72%) was obtained with this catalyst using CH_3OH as alkylating agent, in different catalytic conditions (Figure S8). The other H-ZSM-5(40) and H-ZSM-5(15) catalysts, were featuring 35% and 27% *para*-selectivity, respectively. The particular morphology of the crystals of ZSM-5(75) seems to be the main reason to explain the outstanding *para*-xylene selectivity of this catalyst.

Another evidence that the maximum pore openings of H-ZSM5(75) should be through sinusoidal channel is its abnormal behavior in another catalytic reaction: the alkylation of phenol by *t*-BuOH in liquid phase (unpublished results). H-ZSM5(75) in addition to alkylation products gives dimers and oligomers of isobutene, which are not present with the other ZSM-5 catalysts with Si/Al = 15, 25, and 40 in the solution containing the products of the reaction,[12] as they remained blocked inside the pores of ZSM-5. The size of t-BuOH was measured by the software VESTA[35] and is 0.515 × 0.515 × 0.474 nm, so with widths larger than p-xylene (0.257 × 0.490 × 0.775 nm), which most probably prevents the penetration of t-BuOH into sinusoïdal channels. Furthermore, oligomerization reactions require strong acidity, so the high para-selectivity of H-ZSM5(75) cannot be due to a low Al concentration at the external surface. For all of these reasons, the particular shape of the ZSM-5(75) crystals (a stacking of plate-like crystals) offering the maximum pore openings through sinusoidal channels is the most probable explanation to explain its high para-selectivity. As previously reported, the *para*-xylene selectivity in the toluene methylation is mainly determined by the competition between two reaction rates: that of toluene conversion/xylenes formation and that of xylenes isomerization.[49,50] Moreover, *para*-xylene is known to be the xylene isomer with the fastest intracrystalline diffusion in ZSM-5 zeolite.[51] Additional catalytic tests were performed with H-ZSM-5(75) at a higher temperature and slower flow rate, corresponding to a longer contact time. Working at 425 °C (WHSV = 9.4 $g_{toluene+CH3SH}\ g_{cat}^{-1}\ h^{-1}$) increases toluene and CH_3SH conversions (toluene: from 10% to 20%, CH_3SH: from 30% to 60%), but decreases the *para*-xylene selectivity from 75% to 60%, as it was the case for ZSM-5(15) with an increase of toluene conversion from 27% to 40% and a decrease of *para*-xylene selectivity from 37% to 28% with the increase of temperature from 375 to 425 °C (Figure 3). Higher reaction temperature increases both toluene conversion and xylene isomerization. At 375 °C, by applying a slower flow rate (WHSV = 2.8 $g_{toluene+CH3SH}\ g_{cat}^{-1}\ h^{-1}$), with a longer contact time, toluene and CH_3SH conversions double, but the *para*-xylene selectivity decreased from 75% to 55%. As for the temperature, longer contact time increases both toluene conversion and xylene isomerization. Therefore, the *para*-xylene selectivity in H-ZSM-5(75) catalyst is enhanced by a fast flow rate, so short contact time, and a low temperature reaction.

It can be concluded that the high *para*-xylene selectivity of H-ZSM-5(75) is due to the combination of four factors: the particular morphology of its particles (stacking of plate-like crystallites) maximizing of pore opening through sinusoidal channels favoring the diffusion of *para*-xylene at the expense of *meta*- and *ortho*-xylenes, a low temperature, a fast flow rate, and a low number of acidic sites in the reactor (so a low contact time), which all limit the isomerization of *para*-xylene, the primarily isomer produced inside the pores.

4. Conclusions

The reaction between toluene and methyl mercaptan catalyzed by H-ZSM-5 zeolites with different acidity and morphology was investigated. Based on the experimental results obtained at various reaction parameters, some comments can be made as a conclusion.

- The protonic ZSM-5 zeolites are excellent catalysts for the alkylation of toluene by methyl mercaptan.
- Both reactants were mainly involved in the toluene alkylation, leading to a mixture of methylbenzenes and xylenes, with a larger amount of xylenes.
- The catalytic activity, expressed as reactants (toluene and CH_3SH) conversion, increased with the amount of acid sites of the catalyst, the reaction temperature, and the contact time.
- In opposite, the *para*-xylene selectivity increased with the decrease of the amount of acid sites of the catalyst, the reaction temperature, and the contact time.
- The highest *para*-xylene selectivity (75% at 375 °C) was obtained over H-ZSM-5(75). This catalyst features the lowest acidity and has a particular morphology of particles, which are formed by a stacking of plate-like crystallites, maximizing pore openings through sinusoidal channels, favoring the diffusion of *para*-xylene at the expense of *meta*- and *ortho*-xylenes, which diffuse only in straight channels. These characteristics of H-ZSM-5(75) limited the isomerization of *para*-xylene primarily formed.

As a perspective, processes based on the alkylation reaction could be applied for the simultaneous valorization of the excess of the industrial toluene and the methyl mercaptan recovered from the polluted gases.

Acknowledgments

The authors have nothing to report.

Conflict of Interests

The authors declare no conflict of interest.

Data Availability Statement

The data that support the findings of this study are available in the Supporting Information of this article.

Keywords: Heterogeneous catalysis • Methyl mercaptan • Para-xylene • Toluene alkylation • ZSM-5 zeolites

[1] A. Bayout, C. Cammarano, I. Medeiros-Costa, G. Veryasov, V. Hulea, *Sci. Pollut. Res.* **2024**, *31*, 44669–44690.

[2] E. Huguet, B. Coq, R. Durand, C. Leroi, R. Cadours, V. Hulea, *Appl. Catal. B Environ.* **2013**, *134–135*, 344–348.

[3] V. Hulea, E. Huguet, C. Cammarano, A. Lacarriere, R. Durand, C. Leroi, R. Cadours, B. Coq, *Catal. B Environ.* **2014**, *144*, 547–553.

[4] C. Cammarano, E. Huguet, R. Cadours, C. Leroi, B. Coq, V. Hulea, *Appl. Catal. B Environ.* **2014**, *156–157*, 128–133.

[5] D. He, D. Chen, H. Hao, J. Yu, J. Liu, J. Lu, G. Wan, S. He, K. Li, Y. Luo, *Chem. Eng. J.* **2017**, *317*, 60–69.

[6] D. He, H. Hao, D. Chen, J. Liu, J. Yu, J. Lu, F. Liu, S. He, J. Li, Y. Luo, *Appl. Catal. A Gen.* **2017**, *533*, 66–74.

[7] D. He, Y. Zhao, S. Yang, Y. Mei, J. Yu, J. Liu, D. Chen, S. He, Y. Luo, *Chem. Eng. J.* **2018**, *336*, 579–586.

[8] J. Lu, H. Hao, L. Zhang, Z. Xu, L. Zhong, Y. Zhao, D. He, J. Liu, D. Chen, H. Pu, S. He, Y. Luo, *Appl. Catal. B Environ.* **2018**, *237*, 185–197.

[9] X. Xie, J. Bao, X. Song, X. Sun, P. Ning, C. Wang, F. Wang, Y. Ma, M. Fan, K. Li, *J. Hazard Mater.* **2023**, *442*, 130029

[10] M. Yu, N. Tormene, A. Bolshakov, B. Mezari, A. Liutkova, N. Kosinov, E. J. M. Hensen, *Chem. Commun.* **2021**, *57*, 3323–3326.

[11] R. Watanabe, N. Oba, S. Smith, K. Oshima, M. Kishida, K. Miyake, N. Nishiyama, P. Verma, C. Fukuhara, *RSC Adv.* **2023**, *13*, 21441–21447.

[12] L. Desmurs, C. Cammarano, O. Gimello, A. Galarneau, V. Hulea, *Materials* **2023**, *16*, 6872.

[13] C. Cammarano, E. Gay, A. Finiels, F. Fajula, V. Hulea, *ACS Catal.* **2019**, *9*, 605–609.

[14] A. Bayout, C. Cammarano, I. Medeiros-Costa, G. Veryasov, V. Hulea, *ACS Catal.* **2024**, *14*, 3867–3877.

[15] L. Zhang, N. Liu, C. Dai, R. Xu, G. Yu, B. Chen, N. Wang, *Chem. Synth.* **2022**, *3*, 1–26.

[16] L. Desmurs, A. Galarneau, C. Cammarano, V. Hulea, C. Vaulot, H. Nouali, B. Lebeau, T. J. Daou, C. Vieira Soares, G. Maurin, M. Haranczyk, I. Batonneau-Gener, A. Sachse, *ChemNanoMat* **2022**, *8*, e202200051.

[17] M. Thommes, K. Kaneko, A. Neimark, J. P. Olivier, F. Rodriguez-Reinoso, J. Rouquerol, K. S. W. Sing, *Pure Appl. Chem.* **2015**, *87*, 1051–1069.

[18] P. L. Llewellyn, J. P. Coulomb, Y. Grillet, J. Patarin, G. Andre, J. Rouquerol, *Langmuir* **1993**, *9*, 1852–1856.

[19] A. Galarneau, L. Desmurs, C. Vaulot, H. Nouali, B. Lebeau, T. J. Daou, V. Hulea, C. Cammarano, I. Batonneau-Gener, A. Sachse, *Catalysis Research* **2022**, *2* 29.

[20] P. L. Llewellyn, Y. Grillet, J. Patarin, A. C. Faust, *Microporous Mater.* **1993**, *1*, 247–256.

[21] N. Chakinala, A. G. Chakinala, *Ind. Eng. Chem. Res.* **2021**, *60*, 5331–5351.

[22] D. Dumitriu, C. Guimon, V. Hulea, D. Lutic, I. Fechete, *Appl. Catal. A: Gen.* **2002**, *237*, 211–221.

[23] Y. Xiong, P. G. Rodewald, C. D. Chang, *J. Am. Chem. Soc.* **1995**, *117*, 9427–9431.

[24] M. Guisnet, L. Pinard, *Catal. Rev.* **2018**, *60*, 337–436.

[25] P. Wu, T. Komatsu, T. Yashima, *Microporous Mesoporous Mater.* **1998**, *22*, 343–356.

[26] S. Ilias, A. Bhan, *ACS Catal.* **2013**, *3*, 18–31.

[27] J. W. Park, G. Seo, *Appl. Catal. A: Gen.* **2009**, *356*, 180–188.

[28] S. Svelle, F. Joensen, J. Nerlov, U. Olsbye, K. P. Lillerud, S. Kolboe, M. J. Bjørgen, *Am. Chem. Soc.* **2006**, *128*, 14770–14771.

[29] M. Bjørgen, S. Svelle, F. Joensen, J. Nerlov, S. Kolboe, F. Bonino, L. Palumbo, S. Bordiga, U. Olsbye, *J. Catal.* **2007**, *249*, 195–207.

[30] J. Li, W. Ji, M. Liu, G. Zhao, W. Jia, Z. Zhu, *Microporous Mesoporous Mater.* **2019**, *282*, 252–259.

[31] L. Desmurs, C. Cammarano, G. Ramon, R. Gaumard, T. Mineva, A. Sachse, T. Cacciaguerra, D. Cot, O. Gimello, A. Galarneau, V. Hulea, *ChemCatChem* **2023**, *15*, e202300167.

[32] A. Bayout, C. Cammarano, I. M. Costa, G. Veryasov, A. Sachse, V. Hulea, *J. Catal.* **2024**, *440*,115828.

[33] Q. Chen, J. Liu, B. Yang, B., *Nat. Commun.* **2021**, *12*, 3725,

[34] D. H. Olson, G. T. Kokotailo, S. L. Lawton, S. L. Meier, *J. Phys. Chem.* **1981**, *85*, 2238–2243.

[35] K. Momma, F. Izumi, *J. Appl. Crystallogr.* **2011**, *44*, 1272–1276.

[36] X. Liu, J. Shi, G. Yang, J. Zhou, C. Wang, J. Teng, Y. Wang, Z. Xie, *Commun. Chem.* **2021**, *4*, 107.

[37] M. A. Hernández, A. Abbaspourrad, V. Petranovskii, F. Rojas, R. Portillo, M. A. Salgado, G. Hernández, M.d. l. A. Velazco, E. Ayala, K. F. Quiroz, in *Zeolites and Their Applications* (Eds: M. Nageeb Rashed, P. N. Palanisamy), IntechOpen, London **2018**, Chapter 5, 74–89.

[38] J. Dong, K. Wegner, Y. S. Lin, *J. Membrane Sci.* **1999**, *158*, 17–27.

[39] K. S. W. Sing, R. T. Williams, *Part. Part. Syst. Charact.* **2004**, *21*, 71–79.

[40] R. Gaumard, H. Guesmi, P. Calaminici, A. Köster, J. D. Samaniego Rojas, T. Mineva, *Phys. Chem. C* **2024**, *128*, 7115–7126.

[41] R. D. Shannon, *Acta Cryst* **1976**, *A32*, 751–767.

[42] E. Clementi, D. L. Raimondi, *J. Chem. Phys.* **1963**, *38*, 2686–2689.

[43] R. A. Le Febre, Ph.D. Thesis, Delft University of Technology, Netherlands **1981**.

[44] L. Zhang, N. Liu, C. Dai, R. Xu, G. Yu, B. Chen, N. Wang, *Chem. Synth.* **2022**, *3*, 2.

[45] C. Wang, L. Zhang, X. Huang, Y. Zhu, G. Li, Q. Gu, J. Chen, L. Ma, X. Li, Q. He, J. Xu, Q. Sun, C. Song, M. Peng, J. Sun, D. Ma, *Nat. Commun.* **2019**, *10*, 4348-4356.

[46] X. Huang, R. Wang, X. Pan, C. Wang, M. Fan, Y. Zhu, Y. Wang, J. Peng, *Green Energy Environ.* **2020**, *5*, 385–393.

[47] S. Ezenwa, H. M. Castro, A. J. Hoffman, H. Locht, J. Attebery, D.-Y. Jan, M. Schmithorst, B. Chmelka, D. Hibbitts, R. Gounder, *J. Am. Chem. Soc.* **2024**, *146*, 10666–10678.

[48] L. Desmurs, C. Cammarano, A. Sachse, O. Gimello, T. Gaillard, S. Barberat, S. Blanquer, V. Hulea, A. Galarneau, *Microporous Mesoporous Mater.* **2024**, *377*, 113201.

[49] J. H. Ahn, R. Kolvenbach, S. S. Al-Khattaf, A. Jentys, J. A. Lercher, *ACS Catal.* **2013**, *3*, 817–825.

[50] J. Zhou, Z. Liu, Y. Wang, D. Kong, Z. Xie, *Chem. Sci. Eng.* **2013**, *12*, 103–112.

[51] J. H. Ahn, R. Kolvenbach, S. S. Al-Khattaf, A. Jentys, J. A. Lercher, *Chem. Commun.* **2013**, *49*, 10584.